

Tuning Electron-Transfer Driving Force in Photosynthetic Special Pair Models

Ivana Ramírez-Wierzbicki,^[a, b] Luciano Sanchez Merlinsky,^[a, b] German E. Pieslinger,^[a, c, d] Sofía Domínguez,^[a, b] Leonardo D. Slep,^[a, b] Luis M. Baraldo,^[a, b] and Alejandro Cadranel^{*,[a, b, e, f]}

Visible-light excitation of a family of bimetallic ruthenium polypyridines with the formula $[\text{Ru}^{\text{II}}(\text{tpy})(\text{bpy})(\mu\text{-CN})\text{Ru}^{\text{II}}(\text{py})_4\text{L}]^{\text{n}+}$ ($\text{RuRuL}^{\text{n}+}$), where $\text{L} = \text{Cl}^-$, NCS^- , DMAP and ACN , was used to prepare photoinduced mixed-valence (PI-MV) MLCT states as models of the photosynthetic reaction center. Ultrafast transient absorption spectroscopy allowed to monitor photoinduced IVCT bands between 6000 and 11000 cm^{-1} . Mulliken spin densities resulting from DFT and (TD)DFT computations

revealed the modulation of the charge density distribution depending on the ligand substitution pattern. Results are consistent with PI-MV systems ranging from non-degenerate Class II to degenerate Class III or II/III, with electronic couplings between 1000 and 3500 cm^{-1} . These findings guide the control electron localization-delocalization in charge-transfer/charge-separated excited states, like those involved in the photosynthetic reaction center.

Introduction

In natural photosynthesis, primary charge separation affords a photoinduced mixed valence (PI-MV) system, formed by two redox-active chlorophylls from the special pair that share a single positive charge, $[\text{Chl}_{1\text{A}}\cdot\text{Chl}_{1\text{B}}]^{\text{*+}}$ (Figure 1a).^[1,2] PI-MV systems are those where the mixed-valence core is created in the excited state as a result of a charge transfer process triggered by photoexcitation.^[3–12] Like their ground-state mixed

valence (GS-MV) analogs, PI-MV systems serve as models for electron transfer reactivity, but in the excited state.

In degenerate mixed-valence systems, where the diabatic potential energy surfaces (PES) minima are isoenergetic or redox-symmetric (Figure 1d), electronic coupling plays the major role in defining charge density distribution, which can be finely tuned utilizing different bridges.^[13,14] In non-degenerate systems, where the diabatic PES well depths are non-equivalent (Figure 1e), the free-energy difference or redox asymmetry is crucial.^[15–17] An additional key feature of PI-MV systems, which is absent in GS-MV systems, is the charge-transfer counterpart (CTC), which evolves from the same charge transfer event that creates the PI-MV core. This is decisive, since CTC can alter the free-energy difference between the diabatic PES, biasing charge density distribution, and, with this, the reactivity of the PI-MV system.^[18] For example, in the photosynthetic reaction center, CTC is the separated negative charge initially located on $\text{Chl}_{2\text{A}}^{\text{*}}$ (Figure 1a), an auxiliary chlorophyll from the A branch that is closer to $\text{Chl}_{1\text{A}}$ than to $\text{Chl}_{1\text{B}}$.^[1] This results in the stabilization of an asymmetric distribution of the positive charge density within the PI-MV core, with the oxidizing redox equivalent mostly located on $\text{Chl}_{1\text{A}}$ and oriented towards a tyrosine moiety, which favors hole transfer in Photosystem II.^[19] Thus, in the context of solar-to-chemical transformations, it is imperative to study and control charge density distribution within PI-MV systems as a means to achieve a desired reactivity.

Photoinduced IVCT (PI-IVCT) absorptions, monitored by means of transient absorption spectroscopy (TAS) techniques, provide valuable information about electronic coupling elements and charge density distribution in the excited state. Like for GS-MV systems, the generalized Mulliken-Hush (GMH) model^[20–22] can be applied to PI-MV systems, and equations (1) and (2) can be used to calculate the electronic coupling matrix element H_{DA} for degenerate (Figure 1d) and non-degenerate (Figure 1e) systems upon integration of the PI-IVCT band.

[a] I. Ramírez-Wierzbicki, L. Sanchez Merlinsky, G. E. Pieslinger, S. Domínguez, L. D. Slep, L. M. Baraldo, A. Cadranel
Universidad de Buenos Aires, Facultad de Ciencias Exactas y Naturales, Departamento de Química Inorgánica, Analítica y Química Física, Pabellón 2, Ciudad Universitaria, C1428EHA, Buenos Aires, Argentina
E-mail: acadranel@qi.fcen.uba.ar

[b] I. Ramírez-Wierzbicki, L. Sanchez Merlinsky, S. Domínguez, L. D. Slep, L. M. Baraldo, A. Cadranel
CONICET – Universidad de Buenos Aires. Instituto de Química Física de Materiales, Medio Ambiente y Energía (INQUIMAE), Pabellón 2, Ciudad Universitaria, C1428EHA, Buenos Aires, Argentina

[c] G. E. Pieslinger
CONICET – Universidad de Buenos Aires, Instituto de Química y Fisicoquímica Biológicas (IQUIFIB), Junín 956, C1113AAD, Buenos Aires, Argentina.

[d] G. E. Pieslinger
Donostia International Physics Center, Paseo Manuel de Lardizabal 4, 20018, Donostia, Spain

[e] A. Cadranel
Department Chemie und Pharmazie, Physikalische Chemie Friedrich-Alexander-Universität Erlangen-Nürnberg, Egerlandstraße 3, 91058 Erlangen, Germany

[f] A. Cadranel
Friedrich-Alexander-Universität Erlangen-Nürnberg (FAU), Interdisciplinary Center for Molecular Materials, Egerlandstr. 3, 91058, Erlangen, Germany

Supporting information for this article is available on the WWW under <https://doi.org/10.1002/chem.202402700>

© 2024 The Author(s). Chemistry - A European Journal published by Wiley-VCH GmbH. This is an open access article under the terms of the Creative Commons Attribution Non-Commercial NoDerivs License, which permits use and distribution in any medium, provided the original work is properly cited, the use is non-commercial and no modifications or adaptations are made.

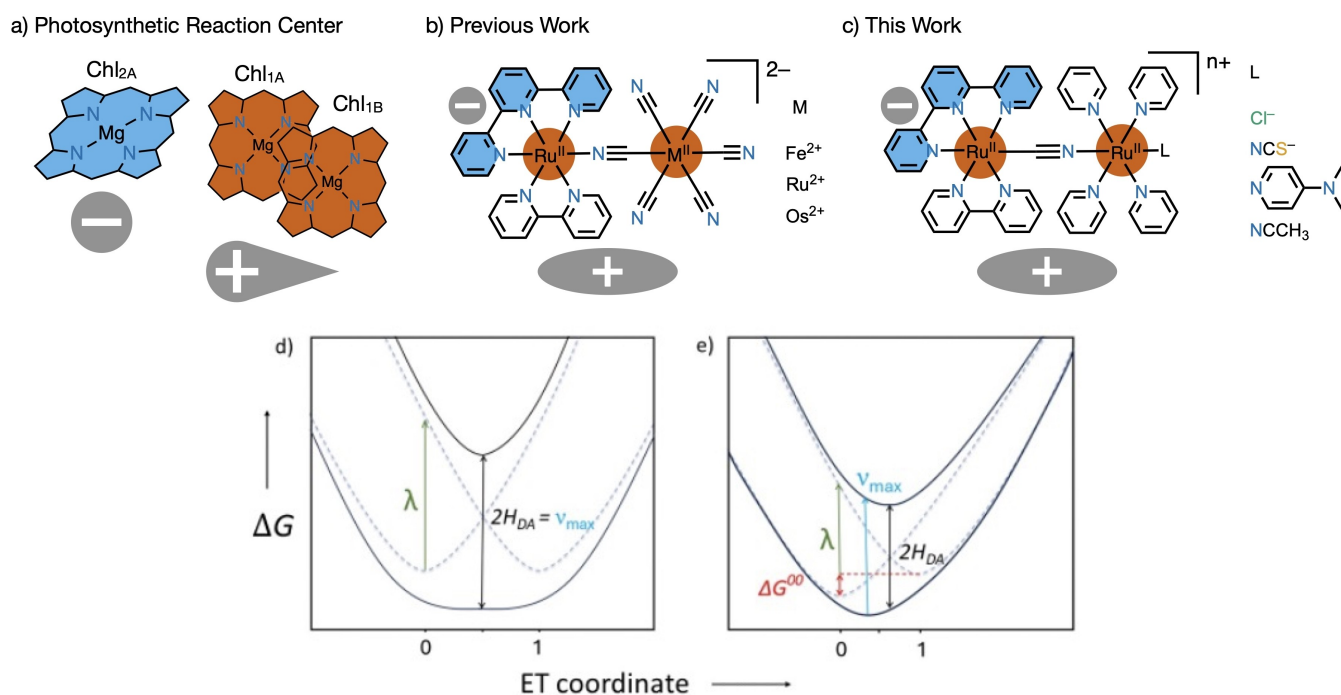


Figure 1. Top: a) PI-MV system in the photosynthetic reaction center, including the oxidized special pair [Chl_{1A}·Chl_{1B}]^{•+} with an asymmetric charge distribution and the Chl_{2A}^{•-} counterpart. b) Sketches of the bimetallic complexes reported previously. c) Sketches of the bimetallic RuRuLⁿ⁺ complexes studied herein. Highlighted similarities are the redox fragments (in orange) and the charge-transfer counterpart (in blue). Bottom: Degenerate (d) and non-degenerate (e) strongly-coupled Class III photoinduced mixed valence systems are simple models of MLCT states in bimetallic RuRuLⁿ⁺.

$$H_{DA} = \frac{|\mu_{DA}|}{er_{DA}} \nu_{max} \quad (1)$$

$$\mu_{DA} = \sqrt{\frac{3hc\epsilon_0 \ln 10}{2000\pi^2 N} \frac{9n}{(n^2 + 2)^2}} \int \frac{\epsilon}{\tilde{\nu}} d\tilde{\nu} \quad (2)$$

There, μ_{DA} is the diabatic transition dipole moment of the PI-IVCT transition, ν_{max} is the energy of the PI-IVCT band, e is the elementary charge, r_{DA} is the donor-acceptor distance, h is Planck's constant, c is the speed of light in vacuum, ϵ_0 is the electrical permittivity of vacuum, N is Avogadro's number, n is the refractive index of the solvent and ϵ is the molar absorption coefficient. Considering that electronic coupling and wavefunction delocalization frequently lead to shorter charge transfer distances than the physical r_{DA} , the value of H_{DA} calculated from eq. (1) is usually an underestimation. For strongly coupled Class III systems, (1) results in simpler expressions (3) and (4) for degenerate (Figure 1d) and non-degenerate systems (Figure 1e), respectively,^[23] which become useful when experimental limitations hinder the detection of the whole band envelope or extinction coefficients are difficult to determine precisely.

$$H_{DA} = \frac{\nu_{max}}{2} \quad (3)$$

$$H_{DA} < \frac{\nu_{max}}{2} \quad (4)$$

Charge transfer excited states in cyanide-bridged {Ru^{II}(tpy)(bpy)-M^{II}(L)₃} compounds (Figure 1b), where {M(L)₃} is a non-chromophoric fragment, are excellent models of the photosynthetic PI-MV system. In these bimetallic complexes, visible light absorption populates MLCT states involving simultaneous i) one-electron oxidation of the {Ru^{II}-M^{II}} fragment, creating a mixed valence core that mimics the special pair of chlorophylls, and ii) one-electron reduction of the tpy ligand, creating a tpy^{•-} CTC directly attached to the Ru ion, which mimics the auxiliary chlorophyll in the photosynthetic reaction center. For example, in photoexcited [Ru^{II}(tpy)(bpy)(μ-CN)M^{II}(CN)₅]²⁻ with M = Fe²⁺, Ru²⁺, Os²⁺, the presence of the excited electron in the transiently reduced tpy^{•-} selectively destabilized the d_π orbitals of the Ru ion directly attached to it. This resulted in an inversion of the electron-donor and acceptor roles relative to the corresponding GS-MV systems, evident from the energy shift of PI-IVCT bands upon changing the redox-asymmetry.^[24–27]

In this contribution, we explore the charge density distribution within the PI-MV systems generated upon visible-light photoexcitation of [Ru^{II}(tpy)(bpy)(μ-CN)Ru^{II}(py)₄L]ⁿ⁺ (RuRuLⁿ⁺), where L = Cl⁻, NCS⁻, DMAP and ACN (Figure 1c), using TAS and DFT/(TD)DFT calculations. The choice of L with different electron-donor or acceptor strengths allowed us to tune charge density distribution. Resulting PI-MV systems spanned from non-degenerate with mostly localized electronic configurations (Figure 1e), where the excited-state CTC imbalances the otherwise degenerate ground-state PES, to degenerate with mostly delocalized electronic configurations (Figure 1d), where the impact of CTC compensates the ground-state redox asymmetry.

Table 1. Photophysical and electrochemical data for RuRuLⁿ⁺ in acetonitrile at room temperature.

| L | Ru _{tb} ^{III/II} E _{1/2} ^[a] /V | Absorption | | Emission (λ _{ex} = 450 nm) | | | |
|------------------|--|---|--|--|-----------------------------------|--------------------|--------------------|
| | | d _π (Ru _{py})→π*(py) ν _{max} /10 ³ cm ⁻¹ | d _π (Ru _{tb})→π*(tpy/bpy) ν _{max} /10 ³ cm ⁻¹ | ν _{max} /10 ³ cm ⁻¹ | Φ _{em} ×10 ⁻³ | τ ₁ /ns | τ ₂ /ns |
| Cl ⁻ | 1.60 | 26.6 | 22.8 (sh) | 14.4 | 0.2 | 2.7 | 6.9 |
| NCS ⁻ | 1.51 | 27.4 | 22.9 (sh) | 13.1 | 0.3 | 2.9 | 7.1 |
| DMAP | 1.60 | 28.3 | 22.2 (sh) | 14.3 | 0.3 | 3.1 | 9.4 |
| ACN | 1.68 | 28.8 | 22.2, 23.6 (sh) | 14.7 | 0.3 | 1.0 | 6.5 |

[a] Extracted from Ref. [28].

The findings reported herein provide guidelines to control charge density distribution in strongly-coupled PI-MV systems, or, in other words, electron localization-delocalization in charge-transfer/charge-separated excited states. This is the first step towards a fine control of excited-state electron-transfer reactivity in multi-component artificial photosynthesis schemes.

Results and Discussion

Photophysics and Excited-State Dynamics

The UV-vis absorption of RuRuLⁿ⁺ in acetonitrile was dominated by MLCT transitions,^[28] and the data was summarized in Table 1. The energy of the d_π(Ru_{py})→π*(py) MLCT increased in the order Cl⁻ < NCS⁻ < DMAP < ACN, tracking the electron-donor or acceptor character of L. The d_π(Ru_{tb})→π*(tpy/bpy) MLCT transitions appeared as shoulders around 22000 cm⁻¹, with the exception of RuRuACN³⁺, for which this transition was resolved and displayed a maximum at 22200 cm⁻¹. The influence of L on the d_π(Ru_{tb})→π*(tpy/bpy) MLCT energy was therefore not clear from these experiments.

All compounds studied here were emissive in acetonitrile at room temperature (Figure 2). Excitation/emission maps are shown in Figures S1-S4, as well as the normalized emission spectra under 22200 cm⁻¹ (450 nm) excitation. No significant dependence of the emission maxima upon photoexcitation wavelength was observed. A correlation was found between the emission maxima and the reduction potential of the Ru^{III/II} couple of the {Ru(tpy)(bpy)} moiety (Table 1), consistent with a ³MLCT origin mainly located on this fragment. Emission quantum yields under 22200 cm⁻¹ (450 nm) excitation were between 2×10⁻⁴ and 3×10⁻⁴, similar to related compounds.^[8,11] Photoluminescence lifetimes were evaluated via TCSPC measurements under the same conditions. Best fits were obtained with biexponential functions involving, in all cases, one lifetime close to 1 ns and another one close to 10 ns (Table 1 and Figures S5-S8). This reveals the presence of two emissive ³MLCT states, ³MLCT_z and ³MLCT_{xy}, consistent with previous reports on RuRuCl²⁺ in DMSO.^[30] Both states include a tpy*⁻ but differ in the configuration of the excited hole (*vide infra*).

In an attempt to observe steady-state emission from both ³MLCT states, explorations at 80 K in a butyronitrile frozen glass matrix were undertaken. Franck-Condon analysis of the

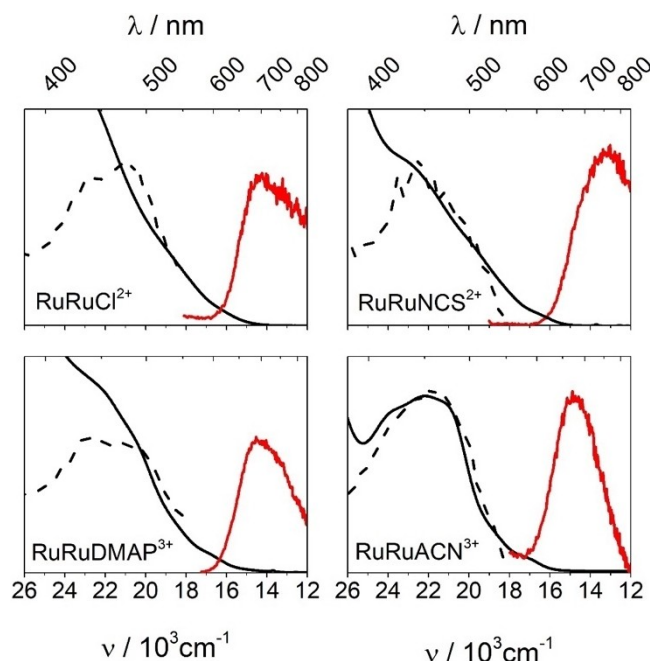


Figure 2. Normalized absorption (black solid lines), excitation (dashed black lines) and emission (red solid line) spectra of RuRuLⁿ⁺ in acetonitrile at room temperature.

observed emission bands was performed,^[31] and good fits were obtained considering a single emitting state (Table S1 and Figures S9-S12). The resulting trend for the extracted E₀₀ followed our observations at room temperature. The Huang-Rhys factor S is a measurement of the nuclear displacement between the equilibrium geometries of the ground and excited states, and small values indicate similar geometries. Therefore, its decrease along the series ACN > DMAP > NCS⁻ > Cl⁻ revealed a progressive nesting of the states involved in the corresponding radiative transitions. This was a consequence of increasing hole delocalization, and was consistent with the strong delocalized character of the excited hole previously reported for RuRuCl²⁺ in DMSO.^[30] Values for ħω between 1200 and 1300 cm⁻¹, typical for C–C and C–N stretching acceptor modes in ruthenium polypyridines,^[32–34] were obtained, except for RuRuCl²⁺ where it is slightly larger. A similar situation was observed for the resulting Δν_{1/2}, around 1200–1400 cm⁻¹ except for L = Cl⁻ with over 1800 cm⁻¹. This might have resulted from

noticeable contributions from the minoritarian emissive state for RuRuCl^{2+} .

To explore the nature of the emitting excited states, we performed nanosecond transient absorption spectroscopy (nsTAS) measurements with vis-NIR detection and 22200 cm^{-1} (450 nm) excitation in acetonitrile at room temperature. Figure S13 shows differential absorption spectra at selected time delays for RuRuL^{n+} . In all cases, three absorption features were observed. First, a negative signal around 20000 cm^{-1} that indicated ground-state population loss. Second, a broad photoinduced absorption between 18000 and 10000 cm^{-1} ascribed to the transiently reduced terpyridine ligand tpy^{*} .^[35–37] For $L = \text{NCS}^-$ and DMAP, this band overlapped with a photoinduced $L \rightarrow \text{Ru}^{\text{III}}$ LMCT transition, also detected in the ground-state absorption spectroscopy of the one-electron oxidized forms of RuRuNCS^{2+} and RuRuDMAP^{3+} .^[28] Third, an intense photoinduced absorption was observed in the NIR between 11000 and 6000 cm^{-1} , that corresponded to a PI-IVCT transition.^[38] Multiwavelength global analysis of the data was performed, and two exponential processes were required to adequately fit

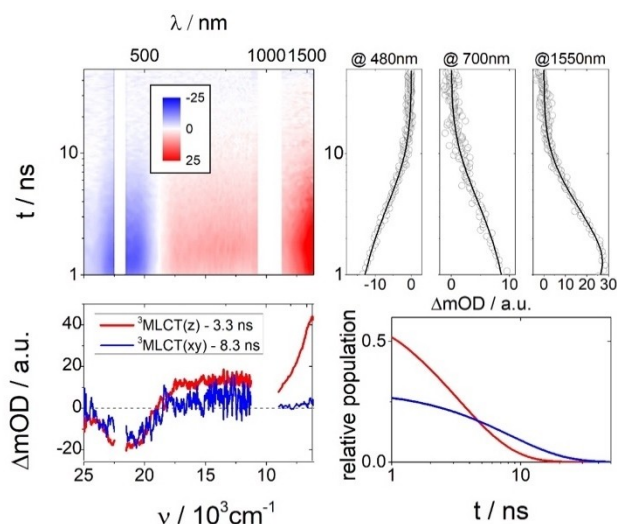


Figure 3. Upper left: differential absorption 3D map obtained from nsTAS experiments on RuRuDMAP^{3+} under 450 nm excitation in acetonitrile at room temperature. Upper right: time absorption profiles (open circles) and corresponding fittings from target analysis (solid lines) using a parallel two-state model. Bottom left: species-associated differential spectra of ${}^3\text{MLCTz}$ (red line) and ${}^3\text{MLCTxy}$ (blue line). Bottom right: relative concentration evolution over time.

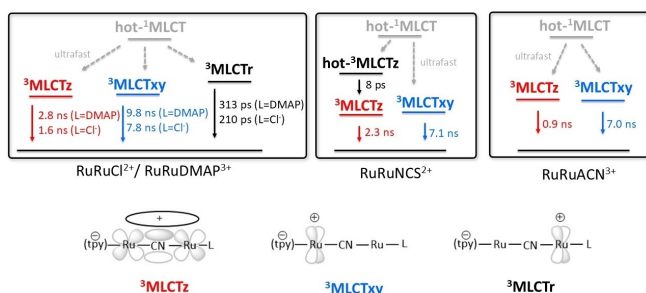


Figure 4. Kinetic target models employed for RuRuL^{n+} (top) and orbital schemes of the excited hole for ${}^3\text{MLCTz}$, ${}^3\text{MLCTxy}$ and ${}^3\text{MLCTr}$ (bottom).

the data. In each case, two nanosecond lifetimes were determined, which matched those obtained from TCSPC measurements. Next, target analysis with parallelly decaying states was conducted to extract species-associated differential spectra (Figures 3 and S14–S16). The kinetic models employed, which considered that both states decay directly to the ground state as revealed by biexponential emission decays, are displayed in Figure 4. For all four RuRuL^{n+} , the species-associated differential spectrum of the shorter-lived excited state showed, along with the ground state bleach and the photoinduced absorptions between 18000 and 10000 cm^{-1} , a PI-IVCT band in the NIR. The presence of the latter is a hallmark of excited-state metal-metal electronic coupling, indicating a significantly delocalized electronic configuration for the excited hole. This was a consequence of a favorable symmetry of the d_{π} orbitals involved along the intermetallic z axis, so these shorter-lived states are labeled ${}^3\text{MLCTz}$. The longest-lived excited state, on the other hand, was NIR-silent. The lack of intense PI-IVCT signatures revealed poor electronic coupling between the Ru ions, stemming from unfavorable symmetry of the d_{π} orbitals involved. The excited hole was therefore localized, and the longest-lived state labeled as ${}^3\text{MLCTxy}$. This behavior was completely analogous to that previously reported for RuRuCl^{2+} in DMSO.^[30]

Next, to shed light onto the kinetic mechanisms that populate the emissive states, we performed femtosecond transient absorption spectroscopy (fsTAS) experiments in acetonitrile at room temperature, with vis-NIR detection and under 22200 cm^{-1} (450 nm) excitation (Figures S15–S18). Considering a 100 fs intersystem crossing,^[39,40] our observation time window involving an approximate resolution of 150 fs started already with triplet populations. For RuRuCl^{2+} and RuRuDMAP^{3+} , it was necessary to consider three exponential processes in the global analysis of the data. Target analysis was undertaken using a model inspired in that previously utilized for RuRuCl^{2+} in DMSO (Figure 4).^[30] It consisted of three parallelly-decaying states, which are populated from the Franck–Condon states in a timescale faster than our time resolution. Two of these states decay in the nanosecond timescale. Their differential absorption profiles and lifetimes matched those obtained from nsTAS for ${}^3\text{MLCTz}$ and ${}^3\text{MLCTxy}$. The third excited state, which decayed in hundreds of picoseconds, featured a differential absorption spectrum showing weak positive signals around 20000 cm^{-1} , instead of a ground-state bleach (Figure S15). Additionally, the photoinduced absorption band in the NIR was absent. This revealed a rather localized configuration for the excited hole, sitting in a d_{π} orbital that was not involved in the $d_{\pi}(\text{Ru}_{\text{tb}}) \rightarrow \pi^*(\text{tpy}/\text{bpy})$ transition and was therefore centered at the $\{\text{Ru}(\text{py})_4\text{L}\}$ fragment. This excited state with a remote electronic configuration was labeled as ${}^3\text{MLCTr}$. For RuRuNCS^{2+} , global analysis of the data also required three exponential processes, but target analysis (Figure S16) was performed using a different kinetic model, depicted on Figure 4. There, our observation window started with ${}^3\text{MLCTxy}$ and a vibrationally excited $\text{hot-}{}^3\text{MLCTz}$. $\text{hot-}{}^3\text{MLCTz}$ underwent vibrational cooling in 8 ps , feeding a thermally relaxed ${}^3\text{MLCTz}$ state which decayed in 2.3 ns to the

Table 2. Difference between the redox potentials of the Ru^{III/II} couples, GS-IVCT and PI-IVCT absorption data, calculated MSD and Ru_{tb}/Ru_L ratios, and ground-state and excited-state electronic couplings for RuRuLⁿ⁺ in acetonitrile at room temperature.

| L | $\Delta E/V^{[a]}$ | GS-IVCT | | | | | PI-IVCT | | | | |
|------------------|--------------------|---|----------------------|-----------------|-------|-------------------------|---|--------------------|-----------------|-------|-------------------------|
| | | $\nu_{\max}/10^3 \text{ cm}^{-1 [a]}$ ($\epsilon/10^3 \text{ M}^{-1} \text{ cm}^{-1 [a]}$) | MSD ^[a,b] | | | H_{DA}/cm^{-1} | $\nu_{\max}/10^3 \text{ cm}^{-1}$ ($\epsilon/10^3 \text{ M}^{-1} \text{ cm}^{-1}$) | MSD ^[b] | | | H_{DA}/cm^{-1} |
| | | | Ru _{tb} | Ru _L | ratio | | | Ru _{tb} | Ru _L | ratio | |
| Cl ⁻ | 0.87 | 10.4 (3.9) | 0.11 | 0.81 | 0.14 | 1590 | 7.0 (5.7) | 0.45 | 0.50 | 0.90 | 3530 |
| NCS ⁻ | 0.75 | 9.7 (4.3) | 0.10 | 0.70 | 0.14 | 1610 | 6.4 (5.2) | 0.57 | 0.36 | 1.58 | < 3200 |
| DMAP | 0.61 | 8.9 (7.5) | 0.11 | 0.73 | 0.15 | 2010 | 6.5 (5.2) | 0.74 | 0.22 | 3.35 | < 3240 |
| ACN | 0.44 | 6.8 (9.5) | 0.46 | 0.48 | 0.96 | 1850, 3400 | 7.9 (3.8), ^[c] 11.2 (2.7) ^[c] | 0.89 | 0.04 | 22.25 | 1320 ^[d] |

[a] Extracted from Ref. [28]. [b] MSD exclusively on the Ru ions, without contributions from additional atoms. [c] Extracted from Gaussian deconvolution (Figure S29). [d] Calculated as the average of the H_{DA} values obtained applying Eq. (2) to the deconvoluted Gaussian functions.

ground state. ³MLCTxy decayed to the ground state in 7.1 ns. For RuRuACN³⁺, a simpler two-state parallel model was sufficient to fit the data (Figures 4). These states corresponded to ³MLCTz and ³MLCTxy, and their lifetimes and differential absorption spectra (Figure S18) agreed with those determined from nsTAS.

PI-IVCT Bands and Charge Density Distribution of ³MLCTz States

Before focusing on the mixed valence properties of RuRuLⁿ⁺ in the excited state, we considered ground-state mixed valence analogs. It was shown that the one-electron oxidized forms of RuRuLⁿ⁺ show intense GS-IVCT bands (Table 2 and Figure 5).^[28] The energy of those transitions was directly related to the redox difference between the metal ions, following the expected trend. DFT and (TD)DFT calculations had an excellent match with the experiment,^[28] providing access to charge density distributions via Mulliken Spin Densities (MSD) (Table 2). Particularly useful was the ratio between the MSD for both Ru ions, which is a better descriptor of charge delocalization than H_{DA} or α^2 and correlates with the energy of the GS- and PI-IVCT bands for cyanide-bridged compounds.^[41] In the ground state, the compound with L=ACN was a Class III or II/III GS-MV system, where the positive charge was equally distributed between the redox fragments despite the structural asymmetry.^[28,42] This implied virtually degenerate diabatic PES minima within this GS-MV system (Figure 1d),^[23] since any significant energy difference would have resulted in an unequal charge distribution despite a strong electronic coupling or Class III or II/III behavior (Figure 1e).^[43,44] The electronic coupling H_{DA} was calculated using eq. (3), and a value of 3400 cm⁻¹ was obtained from the most intense GS-IVCT transition. For L=Cl⁻, NCS⁻ and DMAP, the MSD ratio clearly pointed to an unequal charge distribution, where Ru_L dominated and was therefore the acceptor fragment in the related GS-IVCT transitions. This was consistent with non-degenerate PES in the ground state (Figure 1e). In these cases, the broad shape of the GS-IVCT bands pointed to a Class II behavior. H_{DA} was calculated employing the GMH expressions (1) and (2), considering

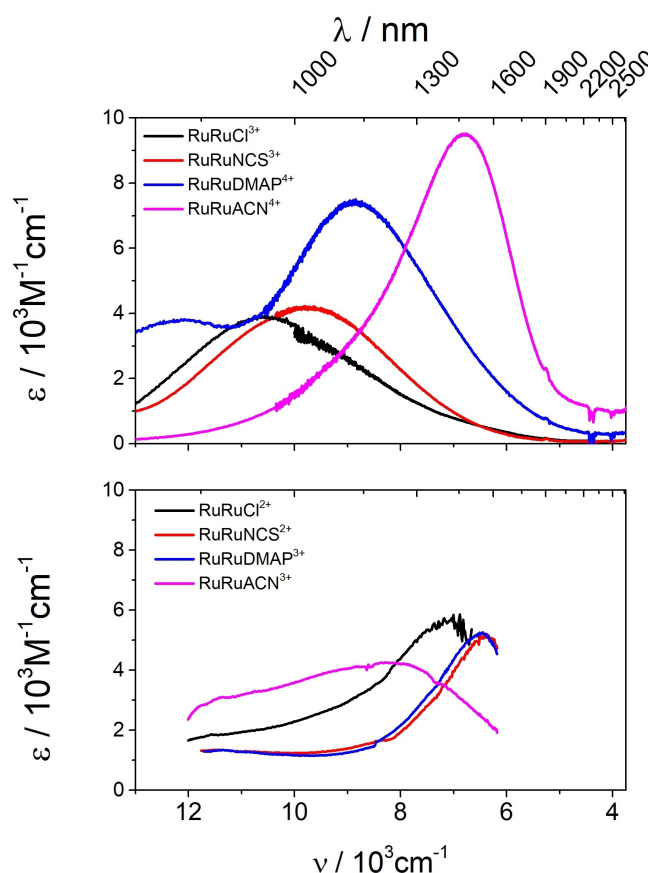


Figure 5. GS-IVCT (top) and PI-IVCT (bottom) absorption bands of RuRuLⁿ⁺ in acetonitrile.

crystallographic donor-acceptor distances of 5.1 Å.^[45] Values of 1590, 1610 and 2010 cm⁻¹ were obtained for L=Cl⁻, NCS⁻ and DMAP, respectively, similar to those reported for related cyanide-bridged Class II systems.^[26,27,46–52]

In the MLCT excited state the picture was different. The presence of the tpy* CTC provokes an inversion of donor-acceptor roles, as observed in related PI-MV systems including the {Ru(tpy)(bpy)} moiety.^[24,25] In this context, PI-IVCT energies were expected to follow the trend L=Cl⁻ < NCS⁻ < DMAP < ACN, in an opposite correlation with the redox difference

between the metal ions ΔE relative to that for GS-IVCT energies. However, TAS experiments revealed a different behavior, with PI-IVCT energies following the order $L = \text{NCS}^- \approx \text{DMAP} < \text{Cl}^- < \text{ACN}$. DFT and (TD)DFT calculations of the lowest triplet states were performed (Tables S2, S4, S6 and S8) to help in the interpretation of the experimental observations. Calculated transitions matched the differential absorption spectroscopy of $^3\text{MLCTz}$ states including PI-IVCT bands (Tables S3, S5, S7 and S9 and Figures S19–S26). Therefore, calculated electronic structures were a good description of $^3\text{MLCTz}$ in these compounds. MSD ratios were obtained and a preliminary analysis indicated, as expected, an opposite trend relative to the ground state (Figure 6 and Table 2).

Considering all the aforementioned facts, we interpreted the PI-IVCT energies according to the following rationale. For $L = \text{NCS}^-$, DMAP and ACN, calculated MSD for Ru_{tb} was larger than that for Ru_{L} , suggesting that in those cases Ru_{tb} was the acceptor in the PI-IVCT transitions. RuRuACN^{3+} showed the most localized configuration for $^3\text{MLCTz}$, with the positive charge density mainly located on Ru_{tb} , and the highest PI-IVCT energy (Figure 6 and Table 2). This PI-MV system clearly belonged to Class II as revealed by a broad PI-IVCT. RuRuDMAP^{3+} also showed a predominantly unbalanced charge distribution, but with larger contributions from Ru_{L} than in RuRuACN^{3+} . As expected for a larger degree of delocalization, the energy of the PI-IVCT was lower than that for $L = \text{ACN}$. Unfortunately, our experimental spectral window precluded the observation of the low-energy flank of the PI-IVCT band for $L = \text{DMAP}$. However, the PI-IVCT band shape was significantly narrower than that for RuRuACN^{3+} , pointing to a Class III or II/III

behavior. For $L = \text{NCS}^-$, also belonging to Class III or II/III, charge distribution was still unbalanced but only slightly, and the MSD ratio approached 1. Stronger delocalization in RuRuNCS^{2+} shifted the PI-IVCT energy to the red, but, simultaneously, energy matching between the PES minima within the PI-MV system afforded and additional boost of H_{DA} , and, with it, a blue-shift of the PI-IVCT band. As a result, this transition appeared at approximately the same energy than that of RuRuDMAP^{3+} . For $L = \text{Cl}^-$, very similar MSD were obtained for both Ru ions, pointing to a quasi-symmetric distribution of charge density. Implicit was a compensation of the ground-state redox asymmetry by the tpy^{*+} counterpart, and a virtual equalization of PES minima. As previously determined in DMSO, $^3\text{MLCTz}$ in this compound also belongs to Class III or II/III. Here the significant blue shift provoked by an excellent energy matching between the PES minima prevailed, and the PI-IVCT transition occurred at an energy slightly higher than that for $L = \text{NCS}^-$ and DMAP. For this classification, it should be noted that the solvent inertial response, i.e. the primary contribution to solvent reorganization, occurs faster than a picosecond,^[53,54] and therefore those PI-MV systems reported here live sufficiently long for solvent molecules to reorient and shape, after vibrational relaxation, a Marcus-Hush scenario like their GS-MV analogues. In this context, inversion of donor-acceptor roles was verified for $L = \text{NCS}^-$, DMAP and ACN, while in $L = \text{Cl}^-$ those roles vanished and PI-MV interactions had only marginal charge-transfer character and result in charge resonance transitions.^[55–57]

Finally, electronic coupling matrix elements H_{DA} were calculated for the GS-MV and PI-MV systems based on RuRuL^{n+}

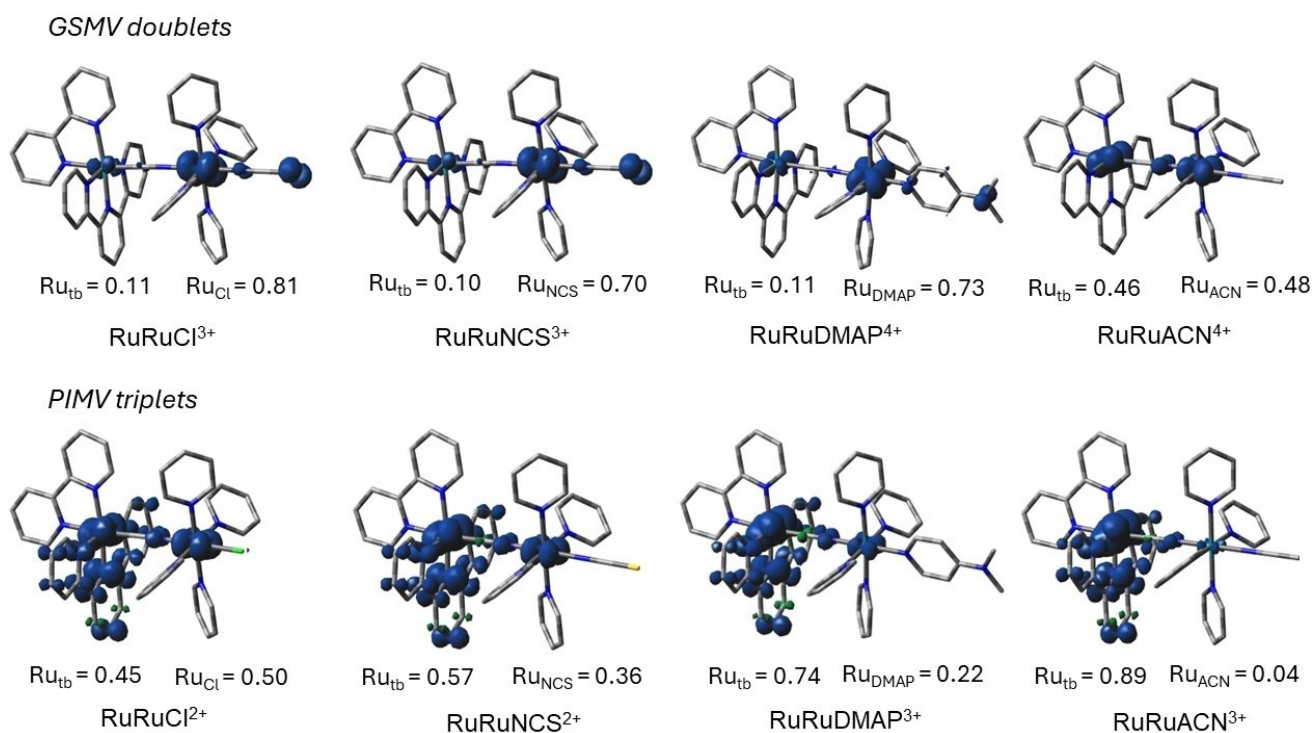


Figure 6. Computed spin density maps (isovalue 0.004) for the lowest-energy doublet GS-MV states (top) and triplet PI-MV states (bottom) in acetonitrile, and calculated Mulliken Spin Densities for each Ru ion.

(Table 2). Molar absorption coefficients of ${}^3\text{MLCTz}$ states were derived from their differential absorption spectra, using eq. (5) and $[\text{Ru}(\text{bpy})_3]^{2+}$ as an actinometer (Figure 5 and Table 2).^[58]

$$\frac{\ln\left(1 - \frac{\Delta A_{wl}^{\text{ref}}}{[\text{ref}]_0 \Delta \epsilon_{wl}^{\text{ref}}}\right)}{\ln\left(1 - \frac{\Delta A_{wl}^{\text{s}}}{[\text{s}]_0 \Delta \epsilon_{wl}^{\text{s}}}\right)} = \frac{\eta^{\text{ref}} \sigma_{\text{ex}}^{\text{ref}}}{\eta^{\text{s}} \sigma_{\text{ex}}^{\text{s}}} \quad (5)$$

There, ΔA_{wl} are the experimental differential absorptions of reference and sample at a specific wavelength wl , $[\text{ref}]_0$ and $[\text{s}]_0$ are reference and sample concentrations, respectively, $\Delta \epsilon$ are the differential molar absorption coefficients of the reference and sample (the last one unknown) at a specific wavelength wl , l is the optical pathlength, η are the quantum efficiency for the population of the corresponding excited state of the reference and sample, and σ are the absorption cross section of reference and sample at the excitation wavelength. According to this procedure, η for the population of ${}^3\text{MLCTz}$ was a key parameter. Since η was related to the branching ratio of the excited-state populations, which were only semi-quantitatively determined in our target analysis, the extinction coefficients obtained were only approximate. Thus, for all Class III or Class II/III compounds, equations (3) and (4) were utilized. For Class II systems, the GMH expressions (1) and (2) were applied.

The results obtained were consistent with our interpretation of PI-IVCT energies. RuRuACN^{4+} in the ground state and RuRuCl^{3+} in the ${}^3\text{MLCTz}$ excited state were degenerate Class III or II/III systems with symmetric charge distributions within the mixed-valence cores, despite asymmetric chemical structures. In this scenario, H_{DA} was around 3500 cm^{-1} . In the other corner, RuRuACN^{3+} in the ${}^3\text{MLCTz}$ excited state and RuRuCl^{4+} in the ground state were typical non-degenerate Class II systems with considerable H_{DA} between 1320 and 2000 cm^{-1} .

This work translates a strategy widely used for the modulation of charge density distribution in the ground state^[59,60] to PI-MV excited states. Interestingly, the effect that the CTC has on the degenerate ground-state Class III or II/III RuRuACN^{4+} is similar to what has been observed for the ligand-based mixed valence system $[\text{Ni}(\text{pdt}^{2-})(\text{pdt}^{\bullet-})]^-$ ($\text{pdt} = 2,3\text{-pyrazinedithiol}$) upon protonation of one of the redox-active moieties, which breaks PES degeneracy and decreases electronic coupling.^[61]

Conclusions

Modulation of charge density distribution within PI-MV states, which is of utmost importance because it determines reactivity of charge-transfer/charge-separated excited states, was demonstrated exploiting ligand substitution in cyanide-bridged bimetallic complexes. The asymmetric influence of the charge-transfer counterpart, like in the photosynthetic special pair, biases the free-energy difference between the diabatic PI-MV states. This bias can be modulated and even compensated using ligands with the necessary electron-donor or acceptor character, resulting in a range of PI-MV systems from non-degenerate

Class II to degenerate Class III or II/III. Further studies exploring the limits of our approach are underway in our labs.

Supporting Information

The authors have cited additional references within the Supporting Information.^[31,62–72]

Acknowledgements

We thank Dirk M. Guldi for providing access to experimental setups. Funding from CONICET (PIP 11220200102757CO and PIBAA 28720210100877CO) and ANPCyT (PICT 2018-00924 and 2019-02410) is acknowledged. I. R. W. and L. S. M. acknowledge doctoral scholarships from CONICET. GEP thanks Prof. Dr. Adrián Roitberg for selflessly sharing his knowledge. GEP, LDS, LMB and AC are members of the research staff of CONICET. Open Access funding enabled and organized by Projekt DEAL.

Conflict of Interests

The authors declare no conflict of interest.

Data Availability Statement

The data that support the findings of this study are available from the corresponding author upon reasonable request.

Keywords: electron transfer · redox asymmetry · transient absorption · solar energy conversion · photosynthesis

- [1] P. D. Harvey, *Can. J. Chem.* **2014**, *92*, 355–368.
- [2] J. R. Reimers, N. S. Hush, in *Artif. Photosynth.*, Wiley, **2005**, pp. 109–126.
- [3] M. H. Chisholm, B. J. Lear, *Chem. Soc. Rev.* **2011**, *40*, 5254–5265.
- [4] M. H. Chisholm, S. E. Brown-Xu, T. F. Spilker, *Acc. Chem. Res.* **2015**, *48*, 877–885.
- [5] M. H. Chisholm, *Coord. Chem. Rev.* **2015**, *282–283*, 60–65.
- [6] J. F. Endicott, Y. J. Chen, *Coord. Chem. Rev.* **2007**, *251*, 328–350.
- [7] J. M. Herrera, S. J. A. Pope, A. J. H. M. Meijer, T. L. Easun, H. Adams, W. Z. Alsindi, X. Z. Sun, M. W. George, S. Faulkner, M. D. Ward, *J. Am. Chem. Soc.* **2007**, *129*, 11491–11504.
- [8] M. G. Fraser, C. A. Clark, R. Horvath, S. J. Lind, A. G. Blackman, X. Sun, M. W. George, K. C. Gordon, *Inorg. Chem.* **2011**, *50*, 6093–6106.
- [9] J. V. Lockard, J. I. Zink, A. E. Konradsson, M. N. Weaver, S. F. Nelsen, *J. Am. Chem. Soc.* **2003**, *125*, 13471–13480.
- [10] J. V. Lockard, J. I. Zink, Y. Luo, M. N. Weaver, A. E. Konradsson, J. W. Fowble, S. F. Nelsen, *J. Am. Chem. Soc.* **2006**, *128*, 16524–16531.
- [11] C. N. Fleming, D. M. Dattelbaum, D. W. Thompson, A. Y. Ershov, T. J. Meyer, *J. Am. Chem. Soc.* **2007**, *129*, 9622–9630.
- [12] I. Ramírez-Wierzbicki, A. Cotic, A. Cadranel, *Encycl. Inorg. Bioinorg. Chem.* **2024**.
- [13] S. S. Isied, A. Vassilian, J. F. Wishart, C. Creutz, H. A. Schwarz, N. Sutin, *J. Am. Chem. Soc.* **1988**, *110*, 635–637.
- [14] W. Kaim, A. Klein, M. Glockle, *Acc. Chem. Res.* **2000**, *33*, 755–763.
- [15] F. Salaymeh, S. Berhane, R. Yusof, R. de la Rosa, E. Y. Fung, R. Matamoros, K. W. Lau, Q. Zheng, E. M. Kober, J. C. Curtis, *Inorg. Chem.* **1993**, *32*, 3895–3908.
- [16] R. De la Rosa, P. J. Chang, F. Salaymeh, J. C. Curtis, *Inorg. Chem.* **1985**, *24*, 4229–4231.

- [17] J. R. Reimers, N. S. Hush, *J. Am. Chem. Soc.* **2004**, *126*, 4132–4144.
- [18] P. S. Oviedo, L. M. Baraldo, A. Cadranel, *Proc. Nat. Acad. Sci.* **2021**, *118*, e2018521118.
- [19] L. Hammarström, S. Styring, *Energy Environ. Sci.* **2011**, *4*, 2379–2388.
- [20] R. J. Cave, M. D. Newton, *Chem. Phys. Lett.* **1996**, *249*, 15–19.
- [21] R. J. Cave, M. D. Newton, *J. Chem. Phys.* **1997**, *106*, 9213–9226.
- [22] B. S. Bruntschwig, C. Creutz, N. Sutin, *Chem. Soc. Rev.* **2002**, *31*, 168–184.
- [23] A. Heckmann, C. Lambert, *J. Am. Chem. Soc.* **2007**, *129*, 5515–5527.
- [24] B. M. Aramburu-Trošelj, P. S. Oviedo, I. Ramírez-Wierzbicki, L. M. Baraldo, A. Cadranel, *Chem. Commun.* **2019**, *55*, 7659–7662.
- [25] B. M. Aramburu-Trošelj, P. S. Oviedo, G. E. Pieslinger, J. H. Hodak, L. M. Baraldo, D. M. Guldi, A. Cadranel, *Inorg. Chem.* **2019**, *58*, 10898–10904.
- [26] A. Cadranel, P. Alborés, S. Yamazaki, V. D. Kleiman, L. M. Baraldo, *Dalton Trans.* **2012**, *41*, 5343–5350.
- [27] A. Cadranel, B. M. Aramburu Trošelj, S. Yamazaki, P. Alborés, V. D. Kleiman, L. M. Baraldo, *Dalton Trans.* **2013**, *42*, 16723–16732.
- [28] S. E. Domínguez, G. E. Pieslinger, L. Sanchez-Merlinsky, L. M. Baraldo, *Dalton Trans.* **2020**, *49*, 4125–4135.
- [29] A. Juris, V. Balzani, F. Barigelli, S. Campagna, P. Belser, A. Zelewsky, *Coord. Chem. Rev.* **1988**, *84*, 85–277.
- [30] P. S. Oviedo, G. E. Pieslinger, L. M. Baraldo, A. Cadranel, D. M. Guldi, *J. Phys. Chem. C* **2019**, *123*, 3285–3291.
- [31] W. R. Roberts, T. N. Rohrabough, R. M. O'Donnell, *J. Visualization* **2021**, 1–13.
- [32] P. G. Bradley, N. Kress, B. A. Hornberger, R. F. Dallinger, W. H. Woodruff, *J. Am. Chem. Soc.* **1981**, *103*, 7441–7446.
- [33] J. V. Caspar, T. D. Westmoreland, G. H. Allen, T. J. Meyer, P. G. Bradley, W. H. Woodruff, *J. Am. Chem. Soc.* **1984**, *106*, 3492–3500.
- [34] G. D. Danzer, J. R. Kincaid, *J. Phys. Chem.* **1990**, *94*, 3976–3980.
- [35] K. Nakamura, *Bull. Chem. Soc. Jpn.* **1972**, *45*, 1943–1943.
- [36] R. M. Berger, D. R. McMillin, *Inorg. Chem.* **1988**, *27*, 4245–4249.
- [37] N. Queyriaux, C. Esmieu, A. K. Gupta, L. Vendier, S. Ott, M. Orio, L. Hammarström, *Eur. J. Inorg. Chem.* **2021**, *2021*, 1263–1270.
- [38] I. Ramírez-Wierzbicki, A. Cotic, A. Cadranel, *ChemPhysChem* **2022**, *23*, 287–288.
- [39] M. Chergui, *J. Chem. Soc. Dalton Trans.* **2012**, *42*, 1772.
- [40] N. H. Damrauer, G. Cerullo, A. Yeh, T. R. Bousie, C. V. Shank, J. K. McCusker, *Chemtracts* **1998**, *11*, 621–625.
- [41] G. E. Pieslinger, A. Cadranel, L. M. Baraldo, *J. Braz. Chem. Soc.* **2020**, *31*, 2360–2370.
- [42] X. L. Liu, Y. Li, Q. D. Xu, Z. Q. Wei, X. T. Wu, T. L. Sheng, *New J. Chem.* **2022**, *46*, 7922–7927.
- [43] P. S. Oviedo, G. E. Pieslinger, A. Cadranel, L. M. Baraldo, *Dalton Trans.* **2017**, *46*, 15757–15768.
- [44] S. Mallick, T. Cheng, L. Chen, M. Meng, Y. Y. Zhang, C. Y. Liu, *Dalton Trans.* **2017**, *46*, 5711–5723.
- [45] A. Cadranel, J. E. Tate, P. S. Oviedo, S. Yamazaki, J. H. Hodak, L. M. Baraldo, V. D. Kleiman, *Phys. Chem. Chem. Phys.* **2017**, *19*, 2882–2893.
- [46] F. W. Vance, R. V. Slone, C. L. Stern, J. T. Hupp, *Chem. Phys.* **2000**, *253*, 313–322.
- [47] L. T. Zhang, X. Q. Zhu, S. M. Hu, Y. X. Zhang, S. D. Su, Y. Y. Yang, X. T. Wu, T. L. Sheng, *Dalton Trans.* **2019**, *48*, 7809–7816.
- [48] G. E. Pieslinger, P. Albores, L. D. Slep, B. J. Coe, C. J. Timpson, L. M. Baraldo, *Inorg. Chem.* **2013**, *52*, 2906–2917.
- [49] K. Barthelmes, M. Jäger, J. Kübel, C. Friebe, A. Winter, M. Wächter, B. Dietzek, U. S. Schubert, *Inorg. Chem.* **2016**, *55*, 5152–5167.
- [50] F. Roncaroli, L. M. Baraldo, L. D. Slep, J. A. Olabe, *Inorg. Chem.* **2002**, *41*, 1930–1939.
- [51] A. Burewicz, A. Haim, *Inorg. Chem.* **1988**, *27*, 1611–1614.
- [52] C. Díaz, A. Arancibia, *Inorg. Chim. Acta* **1998**, *269*, 246–252.
- [53] S. A. Passino, Y. Nagasawa, T. Joo, G. R. Fleming, *J. Phys. Chem. A* **1997**, *101*, 725–731.
- [54] A. T. Yeh, C. V. Shank, J. K. McCusker, *Science* **2000**, *289*, 935–938.
- [55] Y. N. Tan, T. Cheng, M. Meng, Y. Y. Zhang, C. Y. Liu, M. F. Sun, Y. Zheng, P. J. Low, *J. Phys. Chem. C* **2017**, *121*, 27860–27873.
- [56] M. D. Newton, *Chem. Rev.* **1991**, *91*, 767–792.
- [57] K. D. Demadis, C. M. Hartshorn, T. J. Meyer, *Chem. Rev.* **2001**, *101*, 2655–2686.
- [58] P. Müller, K. Brettel, *Photochem. Photobiol. Sci.* **2012**, *11*, 632–636.
- [59] T. Cheng, M. Meng, H. Lei, C. Y. Liu, *Inorg. Chem.* **2014**, *53*, 9213–9221.
- [60] Y. Y. Yang, X. Q. Zhu, J. P. Launay, C. Bin Hong, S. D. Su, Y. H. Wen, X. T. Wu, T. L. Sheng, *Angew. Chem. Int. Ed.* **2021**, *60*, 4804–4814.
- [61] S. R. Kennedy, P. Goyal, M. N. Kozar, H. P. Yennawar, S. Hammes-Schiffer, B. J. Lear, *Inorg. Chem.* **2016**, *55*, 1433–1445.
- [62] A. Cadranel, P. S. Oviedo, G. E. Pieslinger, S. Yamazaki, V. D. Kleiman, L. M. Baraldo, D. M. Guldi, *Chem. Sci.* **2017**, *8*, 7434–7442.
- [63] L. Petit, P. Maldivi, C. Adamo, *J. Chem. Theory Comput.* **2005**, *1*, 953–962.
- [64] R. E. Stratmann, G. E. Scuseria, M. J. Frisch, *J. Chem. Phys.* **1998**, *109*, 8218–8224.
- [65] H. Ishida, S. Tobita, Y. Hasegawa, R. Katoh, K. Nozaki, *Coord. Chem. Rev.* **2010**, *254*, 2449–2458.
- [66] I. H. M. Van Stokkum, D. S. Larsen, R. Van Grondelle, *Biochim. Biophys. Acta Bioenerg.* **2004**, *1657*, 82–104.
- [67] J. J. Snellenburg, S. Liptonok, R. Seger, K. M. Mullen, I. H. M. van Stokkum, *J. Stat. Softw.* **2012**, *49*, 1–22.
- [68] K. M. Mullen, I. H. M. Van Stokkum, *J. Stat. Softw.* **2007**, *18*, 1–46.
- [69] A. Szabo, N. L. Ostlund, **1996**.
- [70] G. Scalmani, M. J. Frisch, *J. Chem. Phys.* **2010**, *132*, 114110.
- [71] J. Tomasi, B. Mennucci, R. Cammi, *Chem. Rev.* **2005**, *105*, 2999–3094.
- [72] H. B. Schlegel, *J. Comput. Chem.* **1982**, *3*, 214–218.

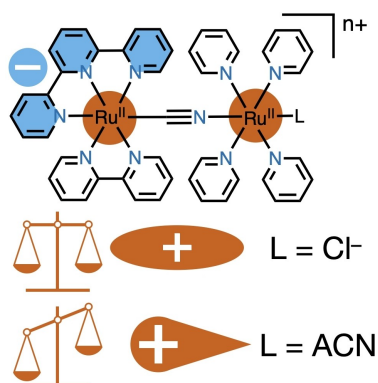
Manuscript received: July 16, 2024

Accepted manuscript online: November 6, 2024

Version of record online: ■■■, ■■■

RESEARCH ARTICLE

In bimetallic $\{(tpy)Ru-Ru(L)\}$, MLCT excited states prepared upon visible light absorption are photoinduced mixed valence systems. This makes them excellent models of the photosynthetic reaction center. In these models, the balance of positive charge density is determined by the tpy radical anion and can be finely controlled by ligand L substitution. Impacts on electronic spectroscopy of photoinduced IVCT bands are discussed with the help of TD-DFT.



*I. Ramírez-Wierzbicki, L. Sanchez Merlinsky, G. E. Pieslinger, S. Domínguez, L. D. Slep, L. M. Baraldo, A. Cadranel**

1 – 9

Tuning Electron-Transfer Driving Force in Photosynthetic Special Pair Models

